ELSEVIER

Journal of Alloys and Compounds 283 (1999) 213–224

Journal of ALLOYS AND COMPOUNDS

Thermodynamic analysis of the hydriding process of Mg–Ni alloys

Kejun Zeng*, T. Klassen, W. Oelerich, R. Bormann

Institute of Materials Research, GKSS-Research Center, Max-Planck-Str., D-21502 Geesthacht, Germany

Received 25 September 1998

Abstract

A consistent set of thermodynamic functions for the Mg–Ni–H system has been developed from experimental data, and the Mg–Ni–H phase diagram has been calculated thermodynamically. The extended ternary solubility of hydrogen in Mg_2Ni, the ternary compound phase Mg_2NiH_4, and the effect of Ni addition on the hydrogen solubility in molten magnesium have been modeled thermodynamically. The ternary solid solution phases were extrapolated from the thermodynamic descriptions of the binary edge systems. The thermodynamic functions of the Mg–Ni–H system have been applied to study the hydriding process of Mg–Ni alloys.

Keywords: Hydrogenation modelling; Mg–Ni alloys; Phase diagram calculations

1. Introduction

Magnesium-based alloys are considered to be the most promising materials for hydrogen storage because of their hydrogen-storage capacity, light weight, the abundance of magnesium in the earth's crust, and low-cost compared with alternative systems. Of all the magnesium-based alloys, Mg_2Ni is the most remarkable due to its relatively high capacity and favorable thermodynamics. It absorbs hydrogen at moderate temperatures and pressures and forms a hydride, Mg_2NiH_4, which contains 3.6 wt.% hydrogen [1]. The hydrogen absorption rate of pure magnesium is greatly improved by alloying with Ni due to the catalytic activity of Ni [2]. However, to achieve a desorption pressure of 1 bar or more, as requested for practical applications, Mg_2NiH_4 has to be heated to at least 240°C. In order to make use of this compound at lower temperatures, ternary elements have been added to Mg_2Ni to improve its hydriding and dehydriding behavior [3–5]. However, the effects of these alloying additions on the stability of the hydride have not yet been clarified.

For a better understanding of experimental results and improvement of the alloy properties, knowledge of the thermodynamic stabilities of the alloy phases and their phase relations in the alloy system is required. Therefore, a thermodynamic study of the phase diagrams of hydrogen-containing Mg–Ni-based systems is currently being carried out by our group in order to provide a basis for designing new Mg–Ni-based hydrogen-storage alloys and to optimize their processing techniques. Based on the thermodynamically assessed constituent binary systems, a thermodynamic description of the Mg–Ni–H system is established in the present work and applied to analyze the hydriding process of Mg–Ni alloys.

2. Experimental

2.1. Ternary phases

2.1.1. τ-Mg_2NiH_4

Of the two intermetallic compounds in the Mg–Ni system, $MgNi_2$ does not react with H_2 at pressures up to 27.6 bar and temperatures up to 350°C. However, Mg_2Ni reacts readily with H_2 at 20.7 bar and 325°C [1]. The product of the reaction is a ternary hydride, Mg_2NiH_4. After several hydriding and dehydriding cycles, it reacts readily with H_2 at pressures as low as 13.8 bar and temperatures as low as 200°C. The reaction is reversible and upon decomposition the original starting material is regenerated. Mg_2NiH_4 can also be formed by the mechanical alloying of pure magnesium and nickel powders (3–5 μm particles) at 310°C in a hydrogen atmosphere of

*Corresponding author. On leave from the Department of Physics, Hunan University, 410082 Changsha, P.R. China. Present address: Department of Electrical and Communications Engineering, Helsinki University of Technology, FIN-02015 TKK, Finland. E-mail: kejun.zeng@hut.fi

0925-8388/99/$ – see front matter
PII: S0925-8388(98)00902-5

8 bar with a purity of 99.9995, because the dissociation pressure is only 3 bar at this temperature [6]. Its actual hydrogen stoichiometry is within the range 3.8–4.0 [1] or 3.88–3.94 [7].

The hydride Mg_2NiH_4 has two crystallographic forms, a high temperature (HT) and a low temperature (LT) modification. Thermal analysis of Mg_2NiH_4 carried out in a thermobalance in a hydrogen atmosphere of 0.933 bar revealed that the reversible transition LT↔HT occurred at 220–245°C and the transition was not accompanied by any change in the hydrogen composition for both structures [8]. However, another investigation found that the transition was due to a small composition change between the LT and HT forms, as revealed by X-ray diffraction, differential thermal analysis and thermogravimetry studies [9]. Noreus and Werner [10] reported that the phase transformation of Mg_2NiH_4(HT) at 235°C was eutectoid, producing not only Mg_2NiH_4(LT) but also a small amount of the less hydrogen containing phase Mg_2NiH_y(LT) with $y \approx 2$. Many investigations have confirmed the transition temperature to be around 237°C [7,9,11–16].

2.1.2. Mg_2NiH_{1-x}

In addition to Mg_2NiH_4, four formulas that look like ternary Mg–Ni–H compounds have been reported in the literature: $Mg_2NiH_{0.3}$ [12], Mg_2NiH [16], $Mg_2NiH_{1.2}$ [17], and $Mg_2NiH_{1.8}$ [18]. In fact, however, these phases are either stable hydrogen dissolved Mg_2Ni ($Mg_2NiH_{0.3}$) or metastable oversaturated phases (the other three), rather than new hydrides. In the present work, only the stable hydrogen dissolved phase is considered and the formula Mg_2NiH_{1-x} is used throughout the paper.

2.2. Phase equilibrium data

No ternary Mg–Ni–H phase diagram has been established in the literature so far. However, some phase equilibrium data have been reported. The ternary solubilities in the solid solution phases (Ni) and (Mg), the intermetallic compound $MgNi_2$, and the binary hydride MgH_2 are very limited and are neglected in this work.

From the pressure–composition isotherms of the Mg_2Ni–Mg–H_2 system, the ratio of hydrogen atoms dissolved in the compound Mg_2Ni to metal atoms, H/(Mg+Ni), was estimated to be about 0.1, i.e. the hydrogen content of Mg_2NiH_{1-x} is about 9.09 at.%, in the temperature range 245–390°C [1,13]. Later, it was confirmed that a hydrogen dissolved Mg_2NiH_{1-x} phase with formula $Mg_2NiH_{\sim 0.3}$ could be obtained by a conventional hydrogenation procedure [12,19]. Mintz et al. [11] studied the solubility of hydrogen in Mg_2Ni by means of X-ray diffraction. Samples containing various amounts of hydrogen were prepared by thermal decomposition of Mg_2NiH_4 at various hydrogen pressures below 0.92 bar. The hydrogen contents of the samples were determined by fusing the alloys at about 1000°C and analyzing quantitatively the amount of evolved hydrogen using gas chromatography. X-ray diffraction measurements of the hydrogen dissolved phase Mg_2NiH_{1-x} yielded the relation between the lattice parameters of the hexagonal unit cell and the hydrogen content, from which the solubility limit of hydrogen in Mg_2Ni was determined to be 8.25 at.%, resulting in the formula $Mg_2NiH_{0.27}$. Therefore, it can be accepted that the hydrogen solubility limit in the Mg_2NiH_{1-x} phase is about 9 at.% in the temperature range around 300°C.

The effects of alloying elements on the hydrogen solubilities in molten magnesium were investigated by Huang et al. [20]. Volumetric measurements were performed at 700°C. A sample of a Mg-based binary alloy with a given content of alloying element was placed in a thin-walled reaction chamber of stainless steel filled with hydrogen at a given pressure. The solubility of hydrogen in magnesium was calculated from the absorbed volume of hydrogen at standard temperature and pressure (0°C and 1 bar). It was found that the addition of nickel increased the hydrogen solubility in molten magnesium. The ternary hydrogen solubility data in molten magnesium by Huang et al. [20] were considered reliable in the present work because the binary hydrogen solubilities in magnesium measured in the same work agree very well with other works where similar experimental procedures were employed (see Ref. [21]).

The formation and dissociation behavior of Mg_2NiH_4 has been the topic of many investigations [22–25]. The experimental pressure data obtained in these works are in good agreement. Hysteresis behavior was observed, with the dissociation pressures being much lower than the formation pressures. The width of the hysteresis became much smaller at lower temperatures. The width of the hysteresis can also depend on the circumstances of the respective measurement. If the kinetics of the reaction are slow, the time to reach equilibrium can be quite long. Therefore, if the measurement points are taken too soon, the measured hysteresis will be larger. Consequently, comparing different pressure–composition isotherms, the smallest hysteresis is the most reliable. Reilly and Wiswall [1] determined the dissociation pressure of Mg_2NiH_4 at temperatures from 274 to 349°C by measuring the pressure–composition isotherms for the Mg_2Ni–H_2 system. The Mg–Ni alloys were prepared in an induction furnace under argon, then pulverized to −25 mesh, and introduced into a stainless steel high-pressure reactor. The alloy samples were hydrided by exposing them to H_2 at about 24 bar and up to 350°C. The hydrided alloys were decomposed by reducing the H_2 over-pressure through the use of an evacuated gas reservoir or by outgassing under a dynamic vacuum. The determined curve of the dissociation pressure of Mg_2NiH_4 lies between the curves of its formation pressures and dissociation pressures determined by other groups [22–25]. The dissociation pressure data of Reilly and Wiswall [1] were taken as the most reliable since the dissociation pressure of the binary hydride MgH_2

Table 1
Thermodynamic properties of the Mg_2NiH_4 phase measured by thermal analysis

ΔH (kJ/mol-H_2)	Experimental conditions	Ref.
−47.28	DSC under H_2 flow, scanning rate unknown; dehydriding	[8]
−56.0	DSC at P_{H_2} = 27 bar, 20°C min^{-1}; hydriding of Mg_2Ni, 200–400°C	[28]
−59.0	DSC at P_{H_2} = 9.9 bar, scanning rate unknown; dehydriding	[29]
−63.1	Isothermal calorimetry at P_{H_2} = 6–8 bar, 301°C, average heat of formation from saturated γ′-Mg_2NiH_{1-x}	[24]
−68.0±3	Calorimetry at P_{H_2} = 6–8 bar before LT→HT transition, H_2 absorption of Mg_2Ni	[7]
−65.8	DTA at P_{H_2} = 1.013 bar, 10°C min^{-1}, dehydriding	[9,27]

measured in the same work agrees excellently with many other experiments (see Ref. [21]).

Using a similar experimental procedure, Buchner et al. [26] measured the pressure–composition isotherms for the (Mg_2Ni+Mg)–H_2 system. The obtained dissociation pressures of Mg_2NiH_4 are very close to the curve of Reilly and Wiswall [1]. The dissociation temperature of Mg_2NiH_4 was also measured at 1 atm hydrogen by other investigators [8,9,14,27], but the temperatures were much higher and seem to be less reliable.

2.3. Thermodynamic data

The thermodynamic properties of Mg_2NiH_4 have been studied by means of thermal analysis [7–9,24,27–29], but the results are scattered (Table 1), with the data determined by DSC [8,28,29] being systematically much smaller. From DSC curves, Hirata [14] derived the enthalpies of hydriding at 30 bar and dehydriding at 1 bar of Mg–Ni alloys with different nickel contents. However, his data are as small as about half of those values listed in Table 1. The reason for the small enthalpy data might be that the reactions were not completed at the high scanning rate (20°C min^{-1}). Post et al. [24] carried out isothermal calorimetry measurement of the heat of formation of the Mg_2NiH_4 phase at 301°C using twin-cell heat-conduction calorimeters of Calvet–Tian design. Temperature and data acquisition were computer-controlled, which greatly facilitates achieving long term (10–50 days) isothermal stability and voluminous data handling/storage/analysis requirements when studying reactions of this type. The heat of formation of HT τ-Mg_2NiH_4 from saturated γ′-Mg_2NiH_{1-x} in hydrogen of 6–8 bar was measured to be −63.1 kJ/mol-H_2, close to the heat exchange when τ was dehydrided at 1.01 bar [9,27] (see Table 1). In another work, Post and Murray [7] measured heat exchange during hydrogen absorption of the intermetallic compound γ-Mg_2Ni at 6–8 bar before the LT↔HT transition. The measured value was −68±3 kJ/mol-H_2. Taking into account the enthalpy for the LT↔HT transition and that for the $Mg_2Ni+H_2 \rightarrow Mg_2NiH_{1-x}$ process (see paragraphs below and Table 2), this value agrees very well with their previous work [24] and the DTA measurements of Selvam et al. [9,27].

Enthalpy values of the phase transition LT↔HT of Mg_2NiH_4 determined by means of DSC are collected in Table 2. Ono et al. [29] performed DSC measurements for several thermal cycles between 200 and 250°C. The transition temperature varied around 235°C within a few degrees only and the heat of transition was measured to be 4.14 kJ/mol-H_2 with a deviation of 3%. Post and Murray [7] carried out both up- and down-scan DSC with very low scanning rates. The data were taken from 68 scans with 11 samples. The enthalpy data for both up- and down-scans are very close and agree excellently with that of Ono et al. [29]. The transition temperature by down-scan is 7°C lower than that by up-scan, indicating a small hysteresis effect. This hysteresis effect was also observed in other investigations [15,30].

The heat of hydrogen solution in the Mg_2Ni phase was measured by Post et al. [24]. While the Mg_2Ni phase was hydrided to Mg_2NiH_{1-x} with $x \approx 0.8$ (6.25 at.% H), the corresponding heat exchange decreased smoothly from about −50 kJ/mol-H_2 at initiation to −41 kJ/mol-H_2. When the hydrogen solubility in the formed Mg_2NiH_{1-x} phase was further increased to the stable maximum limit, the heat exchange was further reduced to about −34 kJ/mol-H_2.

The enthalpy and entropy of the reaction $Mg_2NiH_{1-x}+H_2 \leftrightarrow Mg_2NiH_4$ have been derived by many investigators from the experimental desorption or absorption pressures (Table 3). A Japanese group [23,31,32] reported three

Table 2
Temperature and enthalpy of the phase transition LT↔HT of Mg_2NiH_4 measured by DSC

Temp. (°C)	ΔH (kJ/mol-H_2)	Experimental conditions	Ref.
220–245	3.347±0.2	Under H_2 flow, scanning rate unknown	[8,11]
230	~3.3	At P_{H_2} = 27 bar, 20°C min^{-1}	[28]
240	3.55	No experimental details available	[15]
235	4.14	At P_{H_2} = 9.9 bar, scanning rate unknown	[29]
242	4.16	Up-scan, 5.09°C h^{-1}, P_{H_2} = 6–8 bar	[7]
235	4.15	Down-scan, 2.98°C h^{-1}, P_{H_2} = 6–8 bar	[7]

Table 3
Thermodynamic properties of the Mg_2NiH_4 phase derived from the experimental pressures (J, K, mol-H_2)

ΔH	ΔS	Reaction	Temperature range (°C)	Ref.
−64 430±4184	−122.2±6.3	Desorption	274–349	[1]
−63 000		Desorption	302–356	[26]
−63 600		Desorption	220–320	[31]
−62 500		Desorption	220–320	[32]
−62 500	−119	Absorption	299–375	[22]
−64 600	−122	Desorption	299–350	[22]
−61 900		Absorption	220–320	[23]
−63 180		Desorption	259–320	[23]
−53 230	−104.67	Absorption	240–360	[25]
−72 850	−134.43	Desorption	240–360	[25]

slightly different values for the enthalpy of desorption. Good agreement exists among these data and they agree very well with the thermal analysis data in Refs. [7,9,16,24] (see Table 1), except those by Gross et al. [25] due to their very different pressure data.

3. Thermodynamic modeling

In this paper, the following set of designations will be used for the phases in the Mg–Ni–H system: L-liquid, α-(Mg), β-MgH_2, (Ni), γ-Mg_2Ni, η-$MgNi_2$, γ′-Mg_2NiH_{1-x}, τ-Mg_2NiH_4.

3.1. Phase stabilities of the pure elements

The Gibbs energies of the pure elements versus temperature $G_i^0(T) = G_i(T) - H_i^{SER}$ are represented by Eq. (1):

$$G_i^0(T) = a + bT + cT\ln(T) + dT^2 + eT^{-1} + fT^3 + iT^4 + jT^7 + kT^{-9} \quad (1)$$

The G_i^0 data are referred to the constant enthalpy value of the so-called Standard Element Reference, H_i^{SER}, at 298.15 K and 1 bar as recommended by SGTE (Scientific Group Thermodata Europe) [33]. These reference states are cph Mg, fcc Ni, and gas 0.5H_2. The G_i^0 expressions may be given for several temperature ranges, where the coefficients *a*, *b*, *c*, *d*, *e*, *f*, *i*, *j*, and *k* have different values. The $G_i^0(T)$ functions of the pure elements Mg and Ni were taken from Ref. [33] while those for H_2 were from JANAF [40].

3.2. Binary edge systems

3.2.1. The Mg–Ni system

The thermodynamic description of the Mg–Ni system has recently been evaluated by Jacobs and Spencer [34]. The two intermetallic compounds γ-Mg_2Ni and η-$MgNi_2$ were taken as stoichiometric phases. The insignificant mutual solid solubilities of Mg and Ni were not taken into account. The magnetic behavior of Ni was included. The main features of the Mg–Ni phase diagram assessed by Nayeb–Hashemi and Clark [35] have been reproduced within 34°C and 2.5 at.% (Fig. 1), which is a fair result in view of the fact that Mg is a volatile component.

3.2.2. The Mg–H system

A comprehensive critical assessment has been made of the experimental data of the Mg–H system and a set of thermodynamic functions for the Mg–H system has been optimized by the least squares method [21]. Four different types of stable phases in the Mg–H system were modeled: gas, liquid, solid solution phase α-(Mg), and the stoichiometric compound β-MgH_2. Hydrogen was taken as an ideal gas and the gas phase was treated as an ideal mixture of Mg and H_2. The interstitial solid solution phase cph α-(Mg) was described by a sublattice model $(Mg)_1(H,Va)_{0.5}$. Most of the experimental information is in accordance with the modeling, especially the dissociation pressures of β-MgH_2 at different temperatures, the invariant equilibria, and the hydrogen solubilities in magnesium at 1 atm. The thermodynamic properties of the Mg–H system have been well described at pressures below

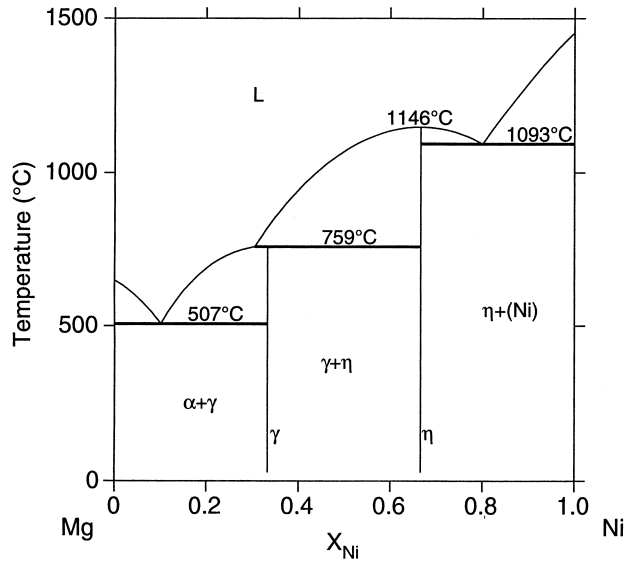

Fig. 1. Calculated Mg–Ni phase diagram [34].

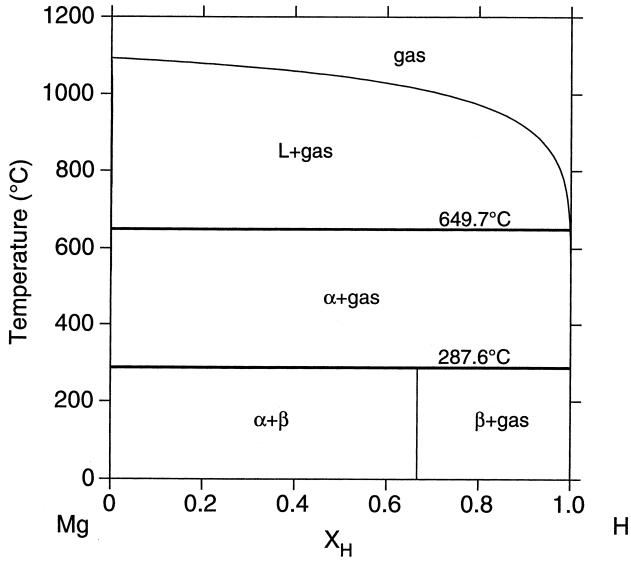

Fig. 2. Calculated Mg–H phase diagram at 1 bar [21].

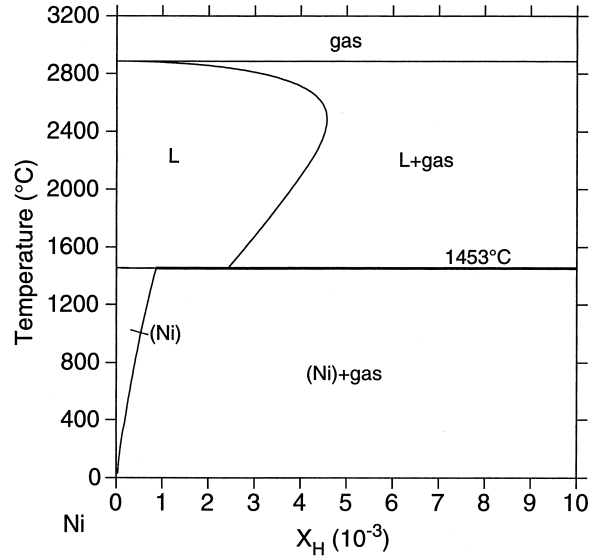

Fig. 3. Calculated Ni–H phase diagram at 1 bar [36].

150 bar. The calculated Mg–H phase diagram at 1 bar is shown in Fig. 2.

3.2.3. The Ni–H system

The thermodynamic properties of the Ni–H binary system have been analyzed using thermodynamic models describing the Gibbs energy of the individual phases [36]. A two-sublattice model $(Ni)_1(H,Va)_1$ was used for the interstitial solution phase fcc-(Ni) and a substitutional solution model was used for the liquid phase. As in the Mg–H system, the gas phase was treated as an ideal solution. The nickel hydride which forms at very high hydrogen pressure (>5000 bar) was not included. Most of the experimental data are well accounted for. Phase equilibria in the system are well described at pressures up to 500 bar. The effect of magnetic ordering in solid nickel on the heat of solution of hydrogen and, consequently, on the hydrogen solubility, is predicted. The calculated Ni–H phase diagram at 1 bar is presented in Fig. 3.

3.3. Modeling of ternary phases

3.3.1. Liquid phase

The liquid phase is described by adopting a substitutional solution model, and its Gibbs energy is expressed as:

$$G_m^L = x_{Mg}G_{Mg}^{0,L} + x_{Ni}G_{Ni}^{0,L} + x_H G_H^{0,L} + RT(x_{Mg}\ln x_{Mg} + x_{Ni}\ln x_{Ni} + x_H \ln x_H) + G_m^{E,L} \quad (2)$$

where x_i is the mole fraction of element i, and $G_{Mg}^{0,L}$ and $G_{Ni}^{0,L}$ are the molar Gibbs energy of Mg and Ni, respectively, in the liquid state and are defined by Eq. (1). $G_H^{0,L}$ is the hypothetical liquid hydrogen evaluated by the present authors [21] from experimental data involving the Mg–H and Ni–H binary liquid phase simultaneously:

$$G_H^{0,L} = (a_H^L + b_H^L T)\ \mathrm{J\ mol^{-1}} + 0.5G_{H_2}^{0,gas} \quad (P = 1.013\ \mathrm{bar}) \quad (3)$$

$G_m^{E,L}$, the excess Gibbs energy, was treated as:

$$G_m^{E,L} = x_{Mg}x_{Ni}L_{Mg,Ni}^L + x_{Mg}x_H L_{Mg,H}^L + x_{Ni}x_H L_{Ni,H}^L + x_{Mg}x_{Ni}x_H L_{Mg,Ni,H}^L \quad (4)$$

where $L_{i,j}^L$ are binary interaction parameters of the i–j system, which are composition dependent according to the Redlich–Kister formalism [37]:

$$L_{i,j}^L = \sum_{n=0}^{m} L_{i,j}^{n,L}(x_i - x_j)^n \quad (5)$$

$L_{i,j}^L$ are taken from the corresponding thermodynamically evaluated binary systems Mg–Ni [34], Mg–H [21], and Ni–H [36]. The parameter $L_{Mg,Ni,H}^L$ in Eq. (4) represents the ternary interaction, which is assumed to have a linear composition dependence according to the expression:

$$L_{Mg,Ni,H}^L = x_{Mg}L_{Mg,Ni,H}^{1,L} + x_{Ni}L_{Mg,Ni,H}^{2,L} + x_H L_{Mg,Ni,H}^{0,L} \quad (6)$$

All three parameters were optimized in the present work.

3.3.2. Solid solutions

The ternary fcc-(Ni) and cph-(Mg) phases were described by a two-sublattice model, assuming that Mg and Ni substitute for each other on the first sublattice and hydrogen and vacant interstitial sites on the second. They were thus represented by the model $(Mg,Ni)_1(H,Va)_b$, with $b=1$ for fcc for crystallographic reasons. For the cph phase, there is an octahedral interstitial site for each metal

atom, but it was assumed that two such sites, situated directly above or below each other, were never occupied simultaneously [38]. Therefore $b=0.5$ for cph.

A thermodynamic model for phases with several sublattices has been used to describe the Gibbs energy for the individual phases [39]. For one mole of formula unit of the Φ phase $(Mg,Ni)_1(H,Va)_b$, this model yields the following expression for the Gibbs energy of each phase:

$$G_m^{\Phi} = y_{Mg}y_H G_{Mg:H}^{0,\Phi} + y_{Mg}y_{Va} G_{Mg:Va}^{0,\Phi} + y_{Ni}y_H G_{Ni:H}^{0,\Phi} + y_{Ni}y_{Va} G_{Ni:Va}^{0,\Phi} + RT((y_{Mg}\ln y_{Mg} + y_{Ni}\ln y_{Ni}) + b(y_H \ln y_H + y_{Va}\ln y_{Va})) + G_m^{E,\Phi} \quad (7)$$

The term y_i represents the site fraction of component i on the sublattice it occupies. The colons separate elements on different sublattices. The parameter $G_{M:Va}^{0,\Phi}$ (M=Mg or Ni) is in fact the Gibbs energy of the pure component M with the same crystal structure as Φ, or $G_M^{0,\Phi}(T)$, as described in Section 3.1; $G_{M:H}^{0,\Phi}$ represents the Gibbs energy of a hypothetical hydride (fcc MgH and NiH, cph $MgH_{0.5}$ and $NiH_{0.5}$) where all interstitial sites are filled with hydrogen. All the $G^{0,\Phi}$ values in Eq. (7) are referred to the standard state SER (see Section 3.1). The parameters $G_{Mg:H}^{0,cph}$ and $G_{Ni:H}^{0,fcc}$ have already been evaluated in the Mg–H [21] and Ni–N [36] binary systems, respectively. The parameters $G_{Mg:H}^{0,fcc}$ and $G_{Ni:H}^{0,cph}$ for metastable fcc in Mg–H and cph in Ni–H systems are adjusted in this work in order to prevent them from becoming stable in the ternary system.

The excess Gibbs energy, $G_m^{E,\Phi}$, is represented by

$$G_m^{E,\Phi} = y_{Mg}y_{Ni}(y_H L_{Mg,Ni:H}^{\Phi} + y_{Va}L_{Mg,Ni:Va}^{\Phi}) + y_H y_{Va}(y_{Mg}L_{Mg:H,Va}^{\Phi} + y_{Ni}L_{Ni:H,Va}^{\Phi}) + y_{Mg}y_{Ni}y_H y_{Va}L_{Mg,Ni:H,Va}^{\Phi} \quad (8)$$

The L^{Φ} parameters represent the interaction energies between two components in the same sublattice dependent on the occupation of the components in the other. The comma separates elements that interact on the same sublattice, and colons separate elements on different sublattices. $L_{Mg,Ni:H}^{\Phi}$ and $L_{Mg,Ni:H,Va}^{\Phi}$ could only be determined from the experimental information on the Mg–Ni–H ternary system, whereas the other three were taken from the binary edge systems.

3.3.3. γ′-Mg_2NiH_{1-x}

The solubility of hydrogen in γ-Mg_2Ni was modeled by the sublattice formula $(Mg)_2(Ni)_1(H,Va)_1$ according to its crystallographic formula $Mg_2NiH_{0.3}$. This model yields the following expression for the Gibbs energy of γ′-Mg_2NiH_{1-x}:

$$G_m^{\gamma'} = y_H G_{Mg:Ni:H}^{0,\gamma'} + y_{Va}G_{Mg:Ni:Va}^{0,\gamma'} + RT(y_H\ln y_H + y_{Va}\ln y_{Va}) + y_H y_{Va}L_{Mg:Ni:H,Va}^{\gamma'} \quad (9)$$

where $G_{Mg:Ni:H}^{0,\gamma'}$ represents the Gibbs energy of a hypothetical hydride $Mg_2Ni_1H_1$, while $G_{Mg:Ni:Va}^{0,\gamma'}$ is actually that of the real binary compound γ-Mg_2Ni, i.e. $G^0(\gamma)$, and $L_{Mg:Ni:H,Va}^{\gamma'}$ is the interaction energy between hydrogen atoms and vacancies on the third sublattice.

3.3.4. τ-Mg_2NiH_4

The hydride τ-Mg_2NiH_4 was treated as a stoichiometric phase. The Gibbs energy of formation was written as a function of T, referring to pure hydrogen gas and the stoichiometric binary compound γ-Mg_2Ni, all at the same temperature:

$$\Delta^f G(\tau) = G^{\circ}(\tau) - G^{\circ}(\gamma) - 2G(H_2) = a^{\tau} + b^{\tau}T + c^{\tau}T\ln T + d^{\tau}T^2 \quad (10)$$

3.3.5. Gaseous phase

Only the species Mg_1, Ni_1 and H_2 were included in the gaseous phase. It was checked in preliminary calculations that other species, such as Mg_1H_2, Mg_1H_1 and Ni_1H_1, are insignificant in the temperature and pressure ranges considered in the present work. Such minority species may also be added from JANAF [40] without changing the present dataset. The gaseous phase was treated as an ideal gas mixture in the calculation. Therefore, Eq. (2) without the excess term G_m^E can be applied to describe its Gibbs energy.

4. Optimization procedure and results

4.1. Parameter selection

The ternary interaction parameters of the liquid in Eq. (6) were fitted to the experimental solubility data of Huang et al. [20]. Because the ternary solubilities in the solid solution phases fcc-(Ni) and cph-(Mg) are very small and no experimental data are available, the ternary parameters are not optimized for them, i.e. the ternary interaction parameters $L_{Mg,Ni:H}^{\Phi}$ and $L_{Mg,Ni:H,Va}^{\Phi}$ in Eq. (8) for both fcc and cph were set to zero, which means that these phases were extrapolated from the constituent binary systems.

No interaction was considered between hydrogen atoms and vacancies on the third sublattice of the hydrogen dissolved phase γ′-Mg_2NiH_{1-x} because there exists only one data for the hydrogen solubility in Mg_2Ni and the parameter $G_{Mg:Ni:H}^{0,\gamma'}$ is sufficient to describe it. That is to say, the parameter $L_{Mg:Ni:H,Va}^{\gamma'}$ in Eq. (9) was not optimized. Although there is no fcc phase in the Mg–H system and no cph phase in the Ni–H system, the parameters $G_{Mg:H}^{0,fcc}$ and $G_{Ni:H}^{0,cph}$ are needed to describe the ternary fcc and cph phases. Thus they were also adjusted in this work.

Due to lack of experimental data on the stability of LT below 230°C and the type of transition LT↔HT (see Section 2.1), the coefficients b^{τ}, c^{τ}, and d^{τ} in Eq. (10) for LT were fixed to the same values optimized for HT, but

coefficient a^{τ} was fitted to the enthalpy change of the transition LT↔HT at 235°C.

4.2. Optimization

The Thermo-Calc program PARROT developed by Jansson [41] was used for the present optimization of the Mg–Ni–H system. A stepwise optimization procedure was designed to ensure the produced parameters were reasonable. It was started by optimizing the thermodynamic functions of Mg_2NiH_4 with respect to the dissociation pressures in Refs. [1,23,26] and the enthalpy of formation of LT [7] and HT [24] by successively taking into account the parameters *a* through *d* in Eq. (10). The obtained parameters were then modified when $G^{0,\gamma'}_{Mg:Ni:H}$ in Eq. (9) was optimized to fit the hydrogen solubility in saturated Mg_2NiH_{1-x} at 297°C [1] and the solution enthalpy at 301°C [24]. Individual values were assigned to the parameters $G^{0,fcc}_{Mg:H}$ and $G^{0,cph}_{Ni:H}$, so that the Mg–H fcc and Ni–H cph phases became metastable in the temperature and pressure ranges of interest. Finally, the whole system was optimized using all the selected experimental data simultaneously. The parameters already obtained were changed slightly in this final step to achieve the best overall fit.

4.3. Results and discussion

The thermodynamic parameters resulting from this least squares procedure are given in Table 4. The equilibrium (dissociation or formation) pressure of Mg_2NiH_4 calculated using these parameters is compared with the experimental formation and dissociation pressures in Fig. 4, where, of the three sets of data of a Japanese group [23,31,32], only that from Ref. [23] was plotted since the three sets of data are very close. The calculated curve agrees excellently with the experimental results of Reilly and Wiswall [1] and lies between the experimental curves for formation and dissociation measured in Refs. [22–25].

Reilly and Wiswall [1] measured the dissociation pressure of Mg_2NiH_4 to be 3.28 bar at 299°C and, as already mentioned in Section 2.1, estimated the hydrogen content of saturated γ'-Mg_2NiH_{1-x} as 9.09 at.%. The vertical section of the Mg–Ni–H phase diagram at 3.28 bar through the line from γ-Mg_2Ni to hydrogen, i.e. the pseudobinary Mg_2Ni–H system, has been calculated in Fig. 5 using the optimized parameters. The hydrogen solubility in the saturated γ'-Mg_2NiH_{1-x} phase is calculated to be 9.07 at.%. The dissociation temperature of Mg_2NiH_4 is predicted at 298.6°C, very close to the experimentally measured 299°C by Reilly and Wiswall [1].

The calculated isothermal section of the Mg–Ni–H phase diagram at 700°C and 1 bar is shown in Fig. 6a. The hydrogen solubility in Mg_2Ni is predicted to be 1.6 at.%. The effect of nickel addition on the hydrogen solubility in molten magnesium has been well accounted for (see Fig. 6b).

The calculated enthalpy changes for different steps of the hydriding process of Mg_2Ni are compared with the experimental results in Table 5. The agreement is excellent. The calculated temperature-dependent enthalpy of dissociation of Mg_2NiH_4 is compared in Fig. 7 with the data derived from the experimental pressures. It agrees excellently with the value from Ref. [1], and the differences from other values are within 2 kJ/mol-H_2. It is worth noting that the calculated curve (full line) in Fig. 7 corresponds to the dissociation equilibrium $Mg_2NiH_4 \leftrightarrow Mg_2NiH_{1-x} + H_2$, where the hydrogen solubility parameter *x* is pressure-dependent and thus temperature-dependent. This curve demonstrates that the thermodynamic modeling method (also called the CALPHAD method) employed in the present work is a very powerful tool for analyzing the thermodynamic properties of a metal–hydrogen system from the equilibrium pressures, as indicated in another paper by the present authors [36].

5. Analysis of the hydriding process of Mg–Ni alloys

It can be concluded from Section 4.3 that the thermodynamic dataset in Table 4 accounts very well for the experimental dissociation pressures of τ-Mg_2NiH_4, solubilities in molten magnesium and γ'-Mg_2NiH_{1-x}, and the thermodynamic properties of hydriding and dehydriding of the intermetallic compound Mg_2Ni. In addition, the thermodynamic description of the Mg–Ni–H system can be applied to analyze the hydriding and dehydriding processes of Mg–Ni binary alloys.

It was observed that when a Mg–Ni binary alloy with the phase mixture of α-(Mg)+Mg_2Ni was hydrided, the first hydride formed was MgH_2 rather than Mg_2NiH_4 [1,26,31]. Later, Post et al. [24] studied the details of the hydriding process of the alloy $Mg_{2.42}Ni$ (Mg–29.24 at.% Ni) at 301°C, which consisted of α-(Mg) and Mg_2Ni phases. It was found that in the beginning the Mg_2Ni phase was hydrided to γ'-$Mg_2NiH_{0.2}$ (6.25 at.% H). Then the α-(Mg) phase reacted with hydrogen to form the magnesium hydride MgH_2. After the α-phase was consumed, the previously formed γ'-$Mg_2NiH_{0.2}$ was further hydrided to γ'-$Mg_2NiH_{0.26}$ (7.98 at.% H) before the ternary hydride Mg_2NiH_4 appeared (For more details, readers are referred to Ref. [24]).

At 301°C, the dissociation or formation pressure of τ-Mg_2NiH_4 is calculated to be 3.47 bar by using the parameters in Table 4. At this pressure and temperature, the isothermal section of the Mg–Ni–H phase diagram is calculated in Fig. 8. This diagram gives interesting information on the hydriding of Mg–Ni binary alloys. When a Mg–Ni alloy with less than 33.3 at.% Ni is exposed to hydrogen at 301°C and 3.47 bar, which is represented by

Table 4
Summary of the thermodynamic parameters describing the Mg–Ni–H system. Values are given in SI units (J, mol, K, Pa) and correspond to 1 mol of formula units of the phases. *Parameters optimized in the present work

Substitutional solution phases (Eq. (2), referred to H^{SER})		
Gas with formula $(Mg,Ni,H_2)_1$, ideal solution		
$G^{gas}_{H_2} = G^{0,gas}_{H_2} + RT\ln(9.8692327\times10^{-6}P)$		
$G^{gas}_{Mg} = G^{0,gas}_{Mg} + RT\ln(9.8692327\times10^{-6}P)$		
$G^{gas}_{Ni} = G^{0,gas}_{Ni} + RT\ln(9.8692327\times10^{-6}P)$		
Liquid with formula $(Mg,Ni,H)_1$		
$G^{0,L}_{H} = +20\,946.25 + 35.31T + 0.5\times G^{0,gas}_{H_2}$		$900<T<6000$
$G^{0,L}_{Mg} = +8202.24 - 8.83693T - 8.01759\times10^{-20}T^7 + G^{0,cph}_{Mg}$		$298.15<T<923$
$= +8690.32 - 9.39216T - 1.03819\times10^{28}T^{-9} + G^{0,cph}_{Mg}$		$923<T<6000$
$G^{0,L}_{Ni} = +16\,414.686 - 9.397T - 3.82318\times10^{-21}T^7 + G^{0,fcc}_{Ni}$		$298.15<T<1728$
$= -9549.775 + 268.598T - 43.1T\ln(T)$		$1728<T<3000$
$L^{0,L}_{Mg,Ni} = -42\,304.49 + 7.45704T$		$298.15<T<6000$
$L^{1,L}_{Mg,Ni} = -15\,611.66 + 9.11885T$		$298.15<T<6000$
$L^{0,L}_{Ni,H} = +5965.3419 - 0.8T$		$298.15<T<6000$
$L^{0,L}_{Mg,Ni,H} = -1.87485553\times10^{4}$	*	$298.15<T<6000$
$L^{1,L}_{Mg,Ni,H} = -2.83801820\times10^{5}$	*	$298.15<T<6000$
$L^{2,L}_{Mg,Ni,H} = +1.07613544\times10^{6}$	*	$298.15<T<6000$
Interstitial solution phases: sublattice model (Eq. (7), referred to H^{SER})		
α-(Mg) with formula $(Mg,Ni)_1(H,Va)_{0.5}$		
$G^{0,cph}_{Mg} = -8367.34 + 143.677875T - 26.1849782T\ln(T) + 4.858\times10^{-4}T^2 - 1.393669\times10^{-6}T^3 + 78\,950T^{-1}$		$298.15<T<923$
$= -14\,130.185 + 204.71854T - 34.3088T\ln(T) + 1.03819\times10^{28}T^{-9}$		$923<T<3000$
$G^{0,cph}_{Ni} = +1046 + 1.255T + G^{0,fcc}_{Ni}$		$298.15<T<3000$
$G^{0,cph}_{Mg:H} = +87\,394.9 - 122.339T + G^{0}(\beta) - 0.75\times G^{0,gas}_{H_2}$		$298.15<T<6000$
$G^{0,cph}_{Ni:H} = +29\,000 + G^{0,fcc}_{Ni} + 0.25\times G^{0,gas}_{H_2}$	*	$298.15<T<6000$
$L^{0,cph}_{Mg,Ni:Va} = +80T$		$298.15<T<6000$
fcc-(Ni) with formula $(Mg,Ni)_1(H,Va)_1$		
$G^{0,fcc}_{Mg} = +2600 - 0.9T + G^{0,cph}_{Mg}$		$298.15<T<3000$
$G^{0,fcc}_{Ni} = -5179.159 + 117.854T - 22.096T\ln(T) - 0.0048407T^2$		$298.15<T<1728$
$= -27\,840.655 + 279.135T - 43.1T\ln(T) + 1.12754\times10^{31}T^{-9}$		$1728<T<3000$
$G^{0,fcc}_{Mg:H} = +51\,000 + G_0(\beta) - 0.5\times G^{0,gas}_{H_2}$	*	$298.15<T<6000$
$G^{0,fcc}_{Ni:H} = -3120.7324 + 180.5062T - 16.2550T\ln(T) + 6.052879\times10^{-4}T^2 + G^{0,fcc}_{Ni} + 0.5\times G^{0,gas}_{H_2}$		$298.15<T<6000$
$L^{0,fcc}_{Mg,Ni:Va} = +80T$		$298.15<T<6000$
The magnetic contribution to the Gibbs energy of fcc-(Ni) is described by:		
$\Delta G^{mo}_{m} = RT\ln(\beta+1)f(\tau)$, where $\tau = T/T_c$		
$f(\tau) = 1 - \frac{1}{A}\left[\frac{79\tau^{-1}}{140P} + \frac{158}{497}\left(\frac{1}{P}-1\right)\left(\frac{\tau^3}{2}+\frac{\tau^9}{45}+\frac{\tau^{15}}{200}\right)\right]$ for $\tau<1$		
$f(\tau) = -\frac{1}{A}\left(\frac{\tau^{-5}}{10}+\frac{\tau^{-15}}{315}+\frac{\tau^{-25}}{1500}\right)$, for $\tau>1$ where		
$A = \frac{518}{1125} + \frac{11\,692}{15\,975}\left(\frac{1}{P}-1\right)$ and P depends on the crystal structure and equals 0.28 for fcc (see Ref. [36])		
γ′-Mg_2NiH_{1-x} with formula $(Mg)_2(Ni)_1(H,Va)_1$ (Eq. (9), refered to H^{SER})		
$G^{0,\gamma'}_{Mg:Ni:Va} = G^{0}(\gamma)$		
$G^{0,\gamma'}_{Mg:Ni:H} = -17\,347.0178 + 42.3496613T + G^{0,\gamma'}_{Mg:Ni} + 0.5\times G^{0,gas}_{H_2}$	*	$298.15<T<6000$
Stoichiometric phases (referred to H^{SER})		
γ with formula Mg_2Ni		
$G^{0}(\gamma) = -82\,211.2 + 571.0183T - 95.992T\ln(T)$		$298.15<T<6000$
η with formula $MgNi_2$		
$G^{0}(\eta) = -74\,136 + 293.9216T - 54.35385T\ln(T) - 0.03329235T^2 - 99T^{-1} + 5.14203\times10^{-6}T^3$		$298.15<T<6000$
β with formula MgH_2		
$G^{0}(\beta) = -108\,422.153 + 495.654655T - 75T\ln(T) - 3.6920685\times10^{-16}T^2 + 5.93903667\times10^{-20}T^3 - 1.7334725\times10^{-8}T^{-1}$		$298.15<T<6000$
τ with formula Mg_2NiH_4		
$G^{0}(\tau) = -144\,753.984 + 350.039372T - 13.7303052T\ln(T) - 0.0130178784T^2 + G°(\gamma) + 2\times G^{0,gas}_{H_2}$	*	$298.15<T<508$
$= -136\,433.984 + 350.039372T - 13.7303052T\ln(T) - 0.0130178784T^2 + G°(\gamma) + 2\times G^{0,gas}_{H_2}$	*	$508<T<2000$

Table 4. Continued.

Symbols	
$G^{0,gas}_{H_2} = -9522.9741 + 78.5273879T - 31.35707T\ln(T) + 0.0027589925T^2 - 7.46390667\times10^{-7}T^3 + 56\,582.3T^{-1}$	$298.15<T<1000$
$= +180.108664 - 15.6128256T - 17.84857T\ln(T) - 0.00584168T^2 + 3.14618667\times10^{-7}T^3 - 1\,280\,036T^{-1}$	$1000<T<2100$
$= -18\,840.1663 + 92.3120255T - 32.05082T\ln(T) - 0.0010728235T^2 + 1.14281783\times10^{-8}T^3 + 3\,561\,002.5T^{-1}$	$2100<T<6000$
$G^{0,gas}_{Mg} = +140\,825.883 - 8.26177982T - 20.96302T\ln(T) + 1.331861\times10^{-4}T^2 - 1.51554617\times10^{-8}T^3 + 5221.91T^{-1}$	$298<T<2900$
$= +141\,959.02 + 20.1923541T - 25.1271T\ln(T) + 0.002179723T^2 - 1.502275\times10^{-7}T^3 - 3\,744\,678T^{-1}$	$2900<T<5400$
$= +458\,455.469 - 794.05688T + 70.54811T\ln(T) - 0.010649025T^2 + 1.716475\times10^{-7}T^3 - 1.996814\times10^{8}T^{-1}$	$5400<T<9200$
$= -315\,972.848 + 423.179252T - 63.73726T\ln(T) - 2.847232\times10^{-4}T^2 + 2.15099667\times10^{-8}T^3 + 6.39436\times10^{8}T^{-1}$	$9200<T<10000$
$G^{0,gas}_{Ni} = +423\,093.837 - 21.4865718T - 24.34001T\ln(T) + 0.0046806645T^2 - 3.40084167\times10^{-6}T^3$	$298<T<400$
$= +423\,608.318 - 43.639632T - 20.26685T\ln(T) - 0.006038615T^2 + 1.2890125\times10^{-6}T^3$	$400<T<800$
$= +419\,186.797 + 15.6323651T - 29.24746T\ln(T) + 0.0021365025T^2 - 1.14496517\times10^{-7}T^3 + 412\,765.95T^{-1}$	$800<T<2600$
$= +419\,346.214 + 9.07992226T - 28.29857T\ln(T) + 0.001646801T^2 - 7.78248167\times10^{-8}T^3 + 785\,084T^{-1}$	$2600<T<5000$
$= +414\,475.627 + 36.7731872T - 31.80175T\ln(T) + 0.0024133565T^2 - 1.0515525\times10^{-7}T^3$	$5000<T<6000$

the dashed line between the alloy and hydrogen in Fig. 8, the hydrogen atoms are first dissolved in the γ-Mg_2Ni phase to γ′-$Mg_2NiH_{0.22}$ (point a in Fig. 8, 6.85 at.% H). Then magnesium in the α-(Mg) phase starts to react with hydrogen to form the hydride β-MgH_2 and the overall composition of the sample enters through point A into the α+β+γ′ three-phase region. This step is controlled by the diffusion of hydrogen atoms in the formed outer layer of γ′-$Mg_2NiH_{0.22}$. If the diffusion of hydrogen atoms in this layer was extremely slow, the hydrogen atoms would accumulate in the surface area and the γ-Mg_2Ni phase would be hydrided directly into τ-Mg_2NiH_4, but this seems not to be the case [24].

After the α-(Mg) phase is consumed at B, the hydriding proceeds with the previously formed γ′-$Mg_2NiH_{0.22}$ being further hydrided in the β+γ′-phase region. When the overall composition of the sample reaches C, the hydrogen content in γ′ approaches the saturation limit γ′-$Mg_2NiH_{0.3}$ (b in Fig. 8). Then, the ternary hydride τ-Mg_2NiH_4 starts to form. Thus, γ-Mg_2Ni is hydrided to its full capacity for hydrogen in two separate steps and the reaction sequences of a Mg–Ni alloy containing less than 33 at.% Ni with hydrogen are as follows:

(i) $Mg_2Ni + H_2 \rightarrow Mg_2NiH_{1-x'}$

(ii) $(Mg) + H_2 \rightarrow MgH_2$

(iii) $Mg_2NiH_{1-x'} + H_2 \rightarrow Mg_2NiH_{1-x}$

(iv) $Mg_2Ni_{1-x} + H_2 \rightarrow Mg_2NiH_4$

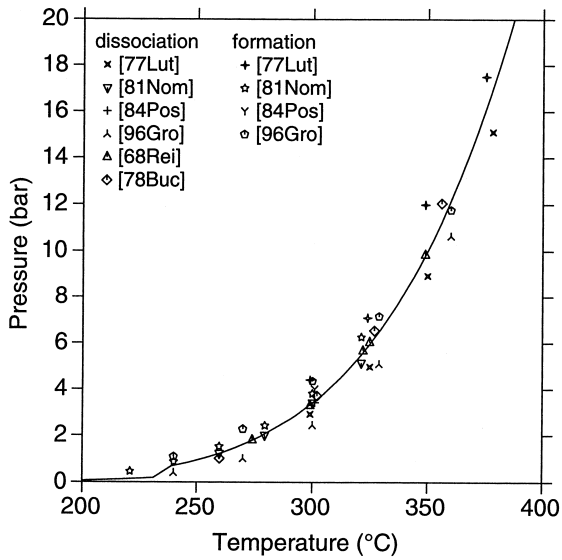

Fig. 4. Calculated equilibrium pressure over Mg_2NiH_4 versus temperature, in comparison with both the experimental dissociation and formation pressures from the literature.

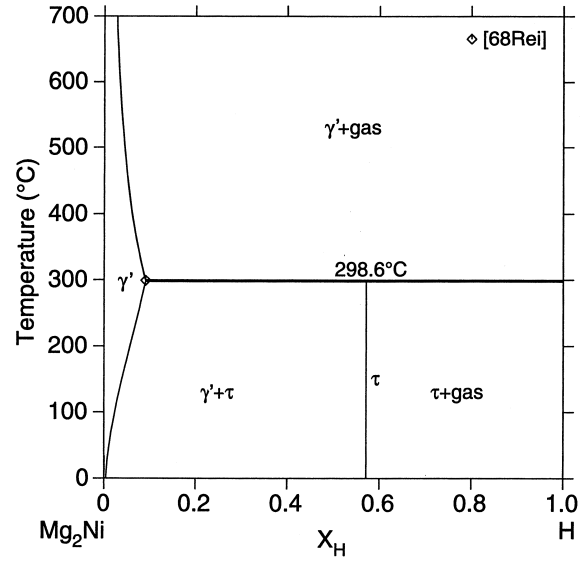

Fig. 5. Calculated vertical section of the Mg–Ni–H phase diagram through the Mg_2Ni–H line at 3.28 bar, showing hydrogen solubility in saturated γ′-Mg_2NiH_{1-x}.

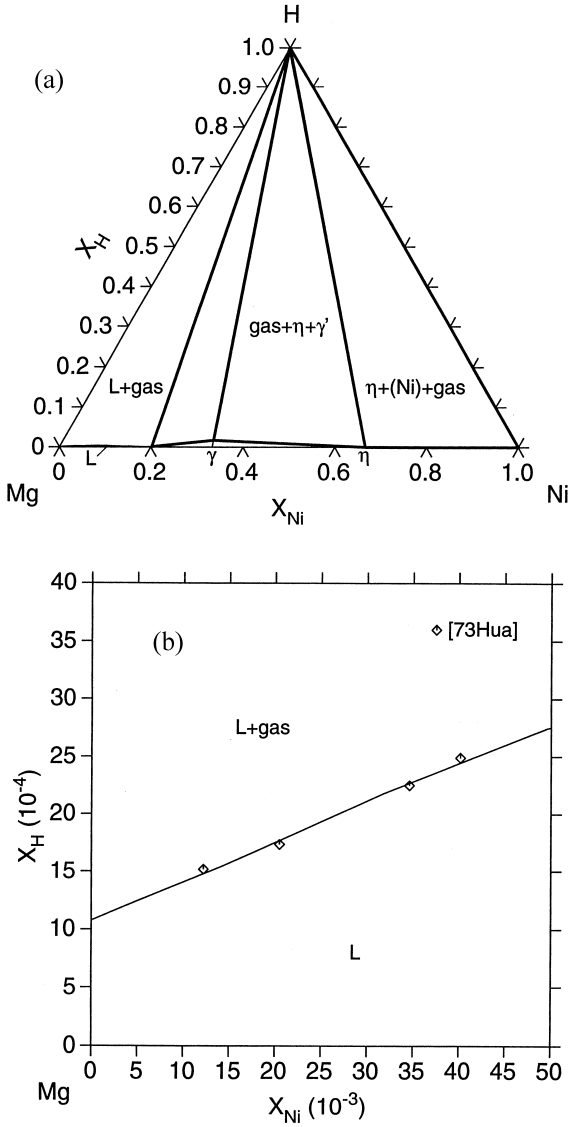

Fig. 6. Calculated isothermal section of the Mg–Ni–H phase diagram at 700°C and 1 bar. (a) The entire section. (b) An enlarged view of the Mg corner in (a), showing the agreement of the calculation with the experimental results with respect to the effects of nickel addition on the hydrogen solubilities in molten magnesium.

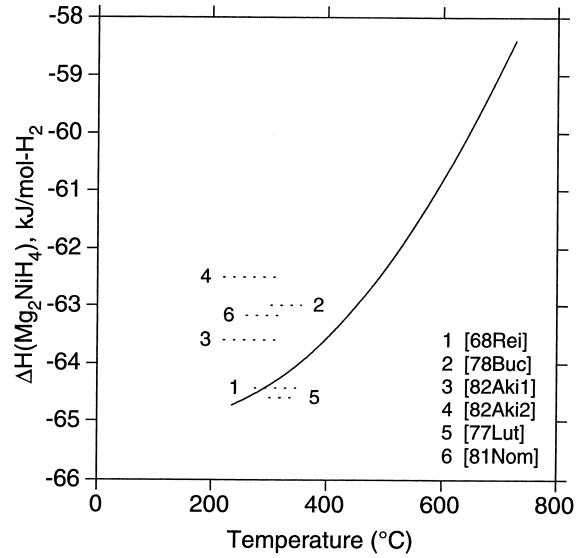

Fig. 7. Calculated enthalpy of dissociation of Mg_2NiH_4 (———) to saturated γ′-Mg_2NiH_{1-x}, compared with literature data derived from the dissociation pressures of Mg_2NiH_4 (- - -).

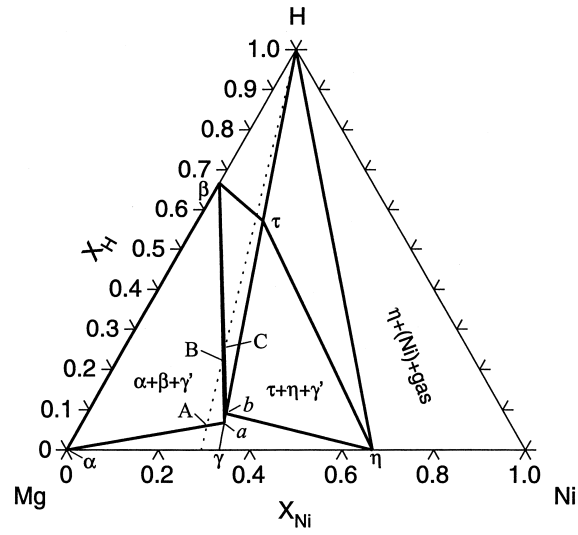

Fig. 8. Calculated isothermal section at 301°C and 3.47 bar. The hydrogen solubility in the saturated γ′-Mg_2NiH_{1-x} phase, when Mg_2NiH_4 decomposes, is calculated to be 9.14 at.%, as shown by point b.

where $x'=0.78$, $x=0.7$ at 301°C, compared with the experimental data of 0.8 and 0.74, respectively, by Post et al. [24]. The smaller hydrogen solubilities in γ′-Mg_2NiH_{1-x} observed experimentally could be attributed to the diffusion kinetics of hydrogen in γ′.

Therefore, the present calculations can predict all the four steps of the hydriding process of an alloy with less than 33.3 at.% Ni and agree with experiments on that, even though β-MgH_2 contains more hydrogen than τ-Mg_2NiH_4,

Table 5
Comparison between calculated and experimental enthalpy changes of hydriding processes

Reaction	Temp. (°C)	ΔH_{calc} (kJ/mol-H_2)	ΔH_{exp} (kJ/mol-H_2)	Ref.
$Mg_2Ni+H_2\rightarrow\gamma'$-$Mg_2NiH_{0.3}$	301	−34.7	−34	[24]
γ′-$Mg_2NiH_{0.3}+H_2\rightarrow Mg_2NiH_4$	301	−64.36	−63.1	[24]
	282	−64.6	−65.8	[27]
$Mg_2Ni+H_2\rightarrow Mg_2NiH_4$	234	−67.2	−68±3	[7]
HT→LT	235	−4.25	−4.15	[7,29]

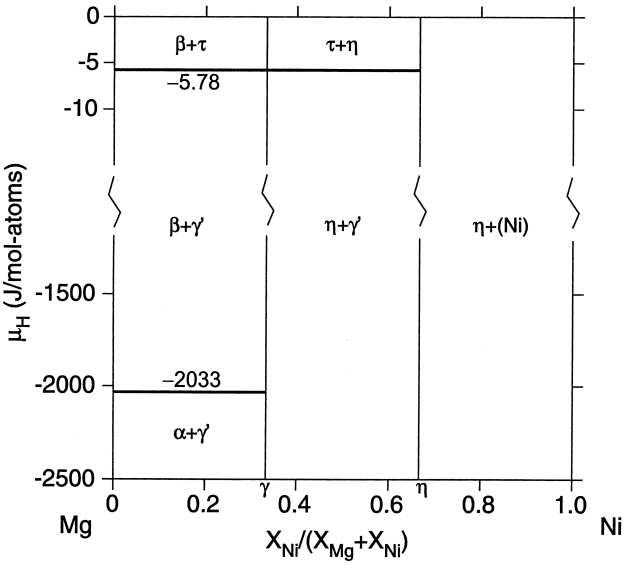

Fig. 9. Predicted phase stability diagram of the Mg–Ni–H system at 301°C and 3.47 bar.

it forms first during hydriding of such an alloy. The reason for this behavior is that the chemical potential of hydrogen in the $\tau+\gamma'+\beta$ three-phase field (-5.78 J/mol-at.) is much less negative than in the $\alpha+\beta+\gamma'$ three-phase field (-2033 J/mol-at.), which is revealed by the calculated stability diagram in Fig. 9. On the other hand, according to Figs. 8 and 9, the dehydriding process of the system will proceed in reverse order of the hydriding process. The Mg_2NiH_4 phase in a hydride mixture of $Mg_2NiH_4+MgH_2$ will decompose first to release hydrogen and produce γ'-Mg_2NiH_{1-x} since the hydrogen potential in it is much higher. This is what was observed experimentally by Post et al. [24].

According to Fig. 8, for a Mg–Ni alloy with a nickel content between 33.3 and 66.7 at.%, the hydriding process is more simple: γ-Mg_2Ni is hydrided directly into the ternary hydride τ, while the η-$MgNi_2$ phase does not take part in the reaction. For a Ni-rich alloy ($X_{Ni}>0.667$), no hydride will be formed because the constituent phase η and (Ni) are in equilibrium with hydrogen. This prediction is in agreement with the experimental result that $MgNi_2$ does not react with H_2 at pressures up to 27.6 bar and temperatures up to 350°C [1].

6. Conclusions

(1) The binary constituent systems Mg–H, Ni–H, and Mg–Ni have been reliably modeled in the temperature and pressure ranges of interest. The Mg–Ni–H ternary system is well described by the obtained thermodynamic parameters above the LT↔HT transition temperature. In order to obtain a better thermodynamic description of the system below the transition temperature, new experiments are required to determine the thermodynamic properties of the low temperature form of τ-Mg_2NiH_4.

(2) The present thermodynamic description of the Mg–Ni–H system can well account for the hydriding process of Mg–Ni alloys with less than 33.3 at.% Ni. The hydriding path of such an alloy is: alloy $\rightarrow\gamma'$-$Mg_2NiH_{1-x'}\rightarrow MgH_2\rightarrow\gamma'$-$Mg_2NiH_{1-x}\rightarrow\tau$-$Mg_2NiH_4$, where $x'>x\geq 0.7$. The reason why MgH_2 forms before Mg_2NiH_4 in these alloys is that the chemical potential of hydrogen in MgH_2 is much more negative than in Mg_2NiH_4.

References

[1] J.J. Reilly, R.H. Wiswall, Inorg. Chem. 7 (1968) 2254.
[2] F.G. Eisenberg, D.A. Zagnoli, J.J.S. III, J. Less-Common Met. 74 (1980) 323.
[3] J.-P. Darnaudery, M. Pezat, B. Darriet, J. Less-Common Met. 92 (1983) 199.
[4] D. Lupu, A. Biris, E. Indrea, Int. J. Hydrogen Energy 7 (1982) 783.
[5] P. Selvam, B. Viswanathan, C.S. Swamy, V. Srinivasan, Int. J. Hydrogen Energy 11 (1986) 169.
[6] M.Y. Song, J. Mater. Sci. 30 (1995) 1343.
[7] M.L. Post, J.J. Murray, J. Less-Common Met. 134 (1987) 15.
[8] Z. Gavra, M.H. Mintz, G. Kimmel, Z. Hadari, Inorg. Chem. 18 (1979) 3595.
[9] P. Selvam, B. Viswanathan, C.S. Swamy, V. Srinivasan, Bull. Mater. Sci. 9 (1987) 21.
[10] D. Noreus, P.-E. Werner, Mater. Res. Bull. 16 (1981) 199.
[11] M.H. Mintz, Z. Gavra, G. Kimmel, Z. Hadari, J. Less-Common Met. 74 (1980) 263.
[12] D. Noreus, P.-E. Werner, Acta Chem. Scand. A 36 (1982) 847.
[13] J. Schefer, P. Fischer, W. Hälg, F. Stucki, L. Schlapbach, J.J. Didisheim, K. Yvon, A.F. Andresen, J. Less-Common Met. 74 (1980) 65.
[14] T. Hirata, Int. J. Hydrogen Energy 9 (1984) 855.
[15] D. Noreus, P.E. Werner, J. Less-Common Met. 97 (1984) 215.
[16] P. Selvam, B. Viswanathan, C.S. Swamy, V. Srinivasan, Thermochim. Acta 125 (1988) 1.
[17] F.J. Liu, G. Sandrock, S. Suda, Z. Phys. Chem. 183 (1994) 163.
[18] S. Orimo, H. Seto, K. Ikeda, M. Nagao, H. Fujii, Physica B 226 (1996) 370.
[19] J.L. Soubeyroux, D. Fruchart, A. Mikou, M. Pezat, B. Darriet, Mater. Res. Bull. 19 (1984) 895.
[20] Y.C. Huang, T. Watanabe, R. Komatsu, in: Proceedings of the 4th International Conference on Vacuum Metallurgy, Tokyo, 1973, p. 176.
[21] K. Zeng, T. Klassen, W. Oelerich, R. Bormann, Int. J. Hydrogen Energy (in press, 1998).
[22] H.M. Lutz, O.D. Pous, in: Proceedings of the 2nd International Congress on Hydrogen in Metals, 2 (1977) 1F5.
[23] K. Nomura, E. Akiba, S. Ono, Int. J. Hydrogen Energy 6 (1981) 295.
[24] M.L. Post, J.J. Murray, J.B. Taylor, Int. J. Hydrogen Energy 9 (1984) 137.
[25] K.J. Gross, P. Spatz, A. Züttel, L. Schlapbach, J. Alloys Comp. 240 (1996) 206.
[26] H. Buchner, O. Bernauer, W. Straub, in: T.N. Veziroglu, W. Seifritz (Eds.), Proceedings of the World Hydrogen Energy Conference, Zürich, 1978, Vol. 3, Pergamon, Oxford, 1978, p. 1677.
[27] P. Selvam, B. Viswanathan, C.S. Swamy, V. Srinivasan, Int. J. Hydrogen Energy 13 (1988) 87.

[28] T. Hirata, T. Matsumoto, M. Amano, Y. Sasaki, J. Phys. F: Met. Phys. 11 (1981) 521.
[29] S. Ono, H. Hayakawa, A. Suzuki, K. Nomura, N. Nishimiya, T. Tabata, J. Less-Common Met. 88 (1982) 63.
[30] A.F. Andersen, E. Andersen, K. Pattersen, Acta Crystallogr. A 37(Suppl. C) (1981) C–152.
[31] E. Akiba, K. Nomura, S. Ono, Y. Minzuno, J. Less-Common Met. 83 (1982) L43.
[32] E. Akiba, K. Nomura, S. Ono, S. Suda, Int. J. Hydrogen Energy 7 (1982) 787.
[33] A.T. Dinsdale, CALPHAD 15 (1991) 317.
[34] M.H.G. Jacobs, P.J. Spencer, J. Chim. Phys. 90 (1993) 167.
[35] A.A. Nayeb-Hashemi, J.B. Clark, in: A.A. Nayeb-Hashemi, J.B. Clark (Eds.), Monograph Series on Alloy Phase Diagrams, Phase diagrams of Binary Magnesium Alloys, ASM International, Metals Park, OH, 1988, p. 219.
[36] K. Zeng, T. Klassen, W. Oelerich, R. Bormann, J. Alloys Comp. 283 (1999) 151.
[37] O. Redlich, A.T. Kister, Ind. Eng. Chem. 40 (1948) 345.
[38] K. Frisk, CALPHAD 15 (1991) 79.
[39] M. Hillert, L.I. Staffanson, Acta Chim. Scand. 24 (1970) 3618.
[40] M.W. Chase, J. Phys. Chem. Ref. Data 14 (Suppl. 1) (1985).
[41] B. Jansson, PhD Thesis, Royal Institute of Technology, Stockholm, Sweden, 1984.